Argon- and krypton-induced reactions at energies of 4–7 MeV/amu

H. C. Britt, B. H. Erkkila, and R. H. Stokes
Los Alamos Scientific Laboratory, Los Alamos, New Mexico 87545*

H. H. Gutbrod
G.S.I., 6100 Darmstadt 1, Germany

F. Plasil and R. L. Ferguson
Oak Ridge National Laboratory, Oak Ridge, Tennessee 37830*

M. Blann*
Nuclear Structure Research Laboratory,† University of Rochester, Rochester, New York 14627

(Received 10 November 1975)

Counter telescope measurements of reactions of $^{40}Ar + ^{109}Ag$ have been made at laboratory energies between 169 and 337 MeV, $^{40}Ar + ^{121}Sb$ at 282 and 340 MeV, and $^{84}Kr + ^{65}Cu$ at 494 and 604 MeV. Measurements and results include elastic scattering, evaporation residue angular distributions and cross sections, fission plus quasifission angular distributions, kinetic energy distributions, and yields versus atomic number. Evaporation residue yields are shown to be consistent with limits predicted by evaporation calculations which include fission competition. Fusion cross sections for the ^{40}Ar plus ^{109}Ag or ^{121}Sb systems are shown to be consistent with the liquid drop limit in terms of the angular momentum at which the fission barrier is estimated to go to zero. Kinetic energies of the fissionlike yields are compared with predicted values.

[NUCLEAR REACTIONS $^{40}Ar + ^{109}Ag$, $^{40}Ar + ^{121}Sb$, $^{84}Kr + ^{65}Cu$, elastic scattering, evaporation residue, fission, quasifission, measured $\sigma(E, \theta)$.]

I. INTRODUCTION

Great interest has centered on the mechanism of heavy ion reactions in the 5–10 MeV/amu energy range. In particular, the question of the conditions necessary to form a compound nucleus has motivated a great deal of work, both experimental and theoretical. This paper reports experimental measurements and possible interpretations for ^{40}Ar and ^{84}Kr induced reactions. The principal target systems were ^{109}Ag and ^{65}Cu, such that the same composite system ($^{149}_{65}Tb$) resulted from different projectiles. Some additional measurements for ^{40}Ar induced reactions of ^{121}Sb are included as well.

Our objective was to make extensive measurements of a few systems, as opposed to broad surveys with limited observation, for each composite system or energy. Measurements of ^{40}Ar induced reactions cover the laboratory energy range of 169 to 340 MeV. Kr measurements were made only at 494 and 604 MeV. Results include the following: elastic scattering, from which total reaction cross sections are deduced; cross sections of products formed by evaporation of a few nucleons from a compound nucleus (hereafter referred to as evaporation residue products, abbreviated ER); and cross sections, kinetic energy, and angular distributions as a function of atomic number for fragments resulting from fission and/or a deep inelastic transfer (quasifission) mechanism.

The ER yields will be compared with limits which result from compound nucleus evaporation theory[1] that include angular momentum dependent fission with rotating liquid drop fission barriers.[2-4] Estimates of the total fusion cross sections (ER plus estimated equilibrium fission) will also be compared with limits imposed by the liquid drop model.

II. EXPERIMENTAL TECHNIQUES

Results to be reported were obtained using ion beams from the Lawrence Berkeley Laboratory, super heavy ion linear accelerator. Measurements were made in a 50 cm scattering chamber using a counter telescope consisting of a gas proportional ΔE counter and a solid state E counter. This device has been described in detail elsewhere.[5] The telescope had an aperture 1 mm $\times$ 4 mm, which was ordinarily 12 cm from the target resulting in an angular acceptance of 0.5°.

The zero angle was determined by measuring elastic scattering at several angles on either side of the nominal zero degree position and by comparing with rates from monitor counters in fixed

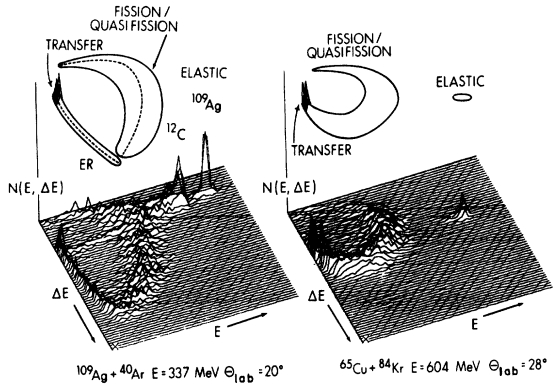

FIG. 1. Contour displays of intensity versus ΔE and E for ^{40}Ar- and ^{84}Kr-induced reactions. The intensity scale is linear. Solid lines above data displays have been added above regions corresponding to different types of yield. The peak below the elastic ^{40}Ar peak on ^{109}Ag is an instrumental effect due to the window of a factor of 100 countdown circuit set on the elastic peak. Angle of measurement and beam energy (laboratory) are indicated on the figure.

positions. To determine absolute cross sections the small angle region of the elastic scattering angular distribution which had zero slope for σ/σ_R was used to calibrate the monitor counters.

The energy resolution observed for elastic peaks was in the range 0.6–2%. Energy calibrations were performed with counters placed at 0° and beam flux attenuators used at the source (to reduce beam intensity), and also with elastic scattering. Additional calibration of both ΔE and E counters was provided by the use of a ^{252}Cf source and by the use of a precision pulse generator to determine slope and intercept of the pulses after analog to digital conversion. Both self-supporting and carbon-backed targets were prepared by vacuum evaporation using 99% enriched isotopes. Silver and copper targets used to obtain evaporation residue data were supported on carbon foils that were 14–20 μg/cm^2 thick. The isotopes were deposited in an area 2 mm high and 1 mm wide with a thickness of 100–200 μg/cm^2. The antimony target consisted of 400 μg/cm^2 of material covering a large area of a 20 μg/cm^2 backing. Fission data were collected by bombarding self-supporting foils of silver and copper that were 150–200 μg/cm^2 thick. The heavy ion beams from the accelerator were collimated with two sets of adjustable slits 0.25 cm wide and 0.5 cm high. The slits were at distances of 38 and 114 cm from the target. An antiscatter aperature 0.5 cm wide and 1.0 cm high was placed 5.0 cm ahead of the target.

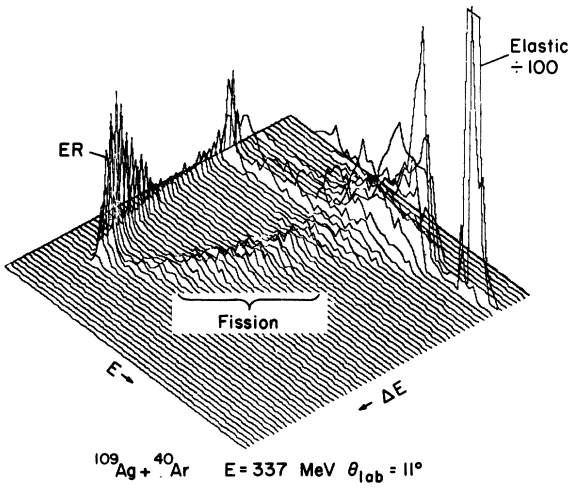

FIG. 2. Contour display for the ^{40}Ar plus ^{109}Ag reaction. The smaller scattering angle allows the ER peak to be observed more clearly.

Beam currents were adjusted such that dead time never exceeded 10% in the data acquisition computer. Maximum currents were of the order of 60 nA for ^{40}Ar ions and 20 nA for ^{84}Kr ions. To reduce dead time a countdown circuit was set for the elastic scattering peak, such that only 1 in 10 or 1 in 100 signals was analyzed by the computer. Windows were set using single channel analyzers, and the necessary scaling factor was adjusted according to the elastic scattering counting rate.

Displays of the data in the E-ΔE plane from one ^{40}Ar + ^{109}Ag and one ^{84}Kr + ^{65}Cu measurement are shown in Figs. 1 and 2. Several types of reaction products are identified in the figures, notably the elastic peaks, evaporation residue, and fission/quasifission groups. Identification of several of these groups is aided somewhat by angular distribution characteristics and kinematics as well as by ionization in the ΔE counter. This point should be somewhat clearer when angular distributions are presented in Sec. III.

III. RESULTS

A. Elastic scattering

Angular distributions for elastic scattering are presented in Fig. 3, as relative cross sections divided by the Rutherford cross section σ/σ_R. The results have been normalized to unity in the flat region of the curves. For strongly absorbing particles, the following semiclassical relationship[6,7] has been proposed between the grazing angular momentum l_c, grazing angle θ_c, and Coulomb radius R_C:

$$l_c = \eta \cot(\tfrac{1}{2}\theta_c) \ , \tag{1}$$

$$l_c(l_c+1) = kR_C(kR_C - 2\eta) \ , \tag{2}$$

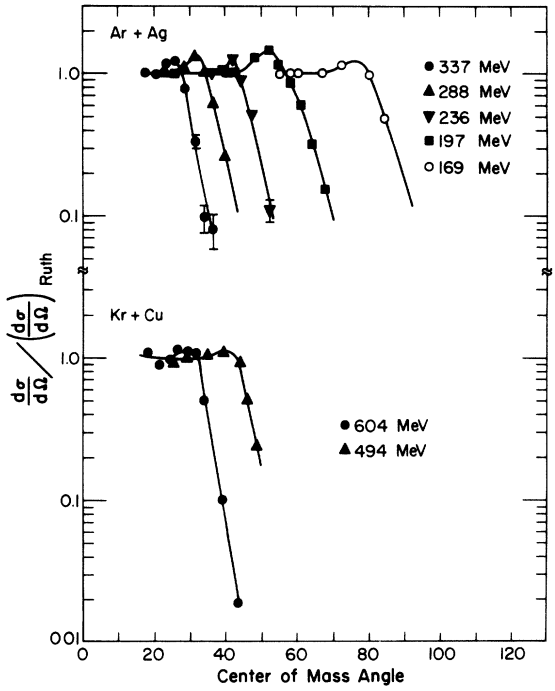

FIG. 3. Elastic scattering angular distributions. Smooth curves have been arbitrarily drawn through the experimental points. Curves are normalized at 1.0 in the region where count rate to Rutherford cross section ratios were constant.

$$\sigma_R = \pi \lambda\!\!\!^{-2}(l_c+1)^2 , \tag{3}$$

where $k = 1/\lambda\!\!\!^{-}$ is the wave number of the projectile and η is the Sommerfield parameter $\eta = Z_1 Z_2 e^2/\hbar v$. Blair showed[6] that l_c could be extracted from elastic scattering angular distributions as the point where $\sigma/\sigma_R = 1/4$. This permits extraction of l_c and R_C without performing an optical model analysis.[7] This has been done and values of l_c, R_C, and reaction cross section σ_R were extracted. These results are presented in Table I. Agreement of l_c between the result of Eqs. (1) and (2) and an optical model analysis was found to be within $\pm 1\hbar$ limit for ^{32}S-induced reactions.[7] For the present data an analysis with the optical model with Woods-Saxon potentials has been performed for the elastic scattering data at 169, 197, 228, and 236 MeV in order to provide another test of Blair's quarter-point rule.[6]

A two parameter search was done starting with the optical potential proposed by Auerbach and Porter which has successfully described elastic heavy ion data.[8] The best-fit parameters are presented in Table II and the computed values for σ_R and $l^{om}_{T=1/2}$ are listed in Table I. The agreement of l_c and σ_R between the results of Eqs. (1) and (2) and the optical model analysis are very good. In Fig. 4 the elastic scattering data are compared with the best-fit optical model calculations.

The major uncertainty in the quantities (σ_R, R_C) deduced from the analysis of elastic scattering data comes from the difficulties in completely separating inelastic from elastic events because of the finite energy resolution of the experiment. The magnitude of this uncertainty was tested in a separate run with a 300 MeV ^{40}Ar beam and the best resolution (0.6%) that we have been able to obtain. A symmetric elastic peak was measured with a low energy tail. The quarter-point analysis was run first using only events in the symmetric peak, next using all events up to 10.6 MeV residual excitation. In the latter case the reaction cross section deduced from quarter-point analysis was 7% lower than the result from the more careful analysis. We think that 7% is a fair upper limit to the errors in our reported reaction cross sections in Table I. A similar analysis for the Kr + Cu reaction at 494 MeV was consistent with this conclusion. In addition, these tests indicated that the apparent variation in geometrical parameters (r_0, a) as a function of energy deduced from both the optical model and quarter-point analyses might be due to the inclusion of varying amounts of inelastic events. Therefore, at this time we cannot make a definite conclusion on whether these apparent variations are real or an artifact resulting from our inability to completely separate out inelastic events.

B. Evaporation residue yields

Angular distributions for products identified as evaporation residues are shown in Fig. 5, and results are summarized in Table I. It may be seen that the ER angular distributions are very strongly forward peaked and show maximum cross sections in excess of 10^4 mb/sr. The strong forward peaking of the ER group is in some cases a limiting factor in the accuracy of experimental results. This is due to the fact that the very high Rutherford cross sections at small angles, together with the physical restrictions of the available scattering chamber and beam optical system, combined to limit the forward angle of observation to 3 or 4°. It was necessary to extrapolate the measured angular distributions to zero degrees prior to multiplying by the $\sin\theta$ factor. This was usually done by an exponential extrapolation of the two lowest angles measured (an upper limit) and by a less steep curve which is qualitatively consistent with the curvature seen in track detector studies which were measured in to zero degrees,[9] and with telescope results measured to smaller angles.[5] The lower portion of Fig. 5

TABLE I. Summary of results.

Projectile Target	^{40}Ar ^{109}Ag					^{40}Ar ^{121}Sb		^{84}Kr ^{65}Cu	
Projectile energy (lab MeV)	169	197	236	288	337	282	340	494	604
Excitation energy (MeV)	71	92	120	158	194	153	197	137	185
Elastic scattering									
η	64.8	60.0	54.9	49.7	45.9	54.4	49.6	67.8	61.2
θ_c	88	65	50	39	32.5	41	32	48	36
k (fm^{-1})	13.1	14.2	15.6	17.2	18.6	17.4	19.1	19.4	21.5
l_c	67	94	118	140	157	145	173	152	188
$l^{om}_{T=1/2}$	66	95	118						
$R_c/(A_1^{1/3}+A_2^{1/3})$ (fm)	1.46	1.47	1.45	1.40	1.38	1.44	1.43	1.44	1.43
σ_R (mb)	859	1410	1830	2110	2270	2210	2600	1950	2430
σ^{om}_R (mb)	848	1452	1880						
Evaporation residue									
σ_I (mb) [a]	285		335		170	280	30	670	300
σ_{II} (mb) [b]	150		285		285	210	370	70	100
σ_{ER} (mb)	435 ± 70	620 [c] ± 90	620 ± 80	670 [c] ± 100	455 ± 50	490 ± 70	500 ± 50	700 ± 300	400 ± 100
σ^{limit}_{ER} (mb) [d]	550		680		480	530	510	960	470
Fission/QF									
σ_f (mb)	20 ± 10	300 [c] ± 100	550 ± 150	600 [c] ± 150	520 ± 150	600 [h]		690 [e] ± 100	1160 [e] ± 150
FWHM (Z)	~11		~17		~20			~17	~17
σ_{QF} (mb) [f]	45 ± 20		370 ± 180		700 ± 350				
General									
σ_{fusion} (mb)	455 ± 70	920 ± 140	1170 ± 170	1270 ± 180	975 ± 160	1130 ± 200		1390 [e] ± 320	1560 [e] ± 180
l_{crit} ($\hbar$)	49 ± 4	76 ± 6	94 ± 7	108 ± 8	103 ± 8	104 ± 10		128 ± 15	150 ± 9
σ_{fusion}/σ_R	0.54 ± 0.08	0.65 ± 0.07	0.64 ± 0.07	0.60 ± 0.07	0.51 ± 0.05				
$\Delta\sigma$ [g]	350 ± 80		290 ± 160		600 ± 200			560 ± 320	870 ± 180

[a] ER cross section below lowest angle of measurement.
[b] ER cross section within range of measured angles.
[c] Results reported in Ref. 10.
[d] ER cross section from exponential extrapolation.
[e] Results may include quasifission.
[f] Estimated quasifission cross sections as shown in Fig. 6.
[g] Difference between total reaction cross section from elastic scattering and sum of measured channels.
[h] From Ref. 34.

TABLE II. Optical model parameters for the elastic scattering of ^{40}Ar on ^{109}Ag.

E_{lab}(^{40}Ar)	V (MeV)	r_v (fm)	a_v (fm)	W (MeV)	r_w (fm)	a_w (fm)
169	41.8	1.25	0.51	8	1.34	0.39
197	41.8	1.25	0.51	8	1.44	0.19
228	41.8	1.26	0.51	8	1.44	0.29
236	41.8	1.21	0.51	8	1.36	0.45

shows the angular distributions multiplied by $\sin\theta$, from which the integrated ER cross sections were deduced. It may be seen that for most of the argon cases the majority of the cross section was measured, while for Kr cases most of the cross section was extrapolated. Table I shows the cross sections which were in the extrapolated region (σ_I), those which were in the measured region (σ_{II}), and the estimated ER cross sections. The upper limit due to the exponential extrapolation is also shown. Error estimates were based on a consideration of measured versus extrapolated cross sections, and on differences between the results of the two modes of extrapolation. Results of earlier measurements[10] are also summarized in Table I.

C. Fission and quasifission distributions

Regions of the E-ΔE plane containing fissionlike events are identified in Figs. 1 and 2. Figure 6 is the result of a very long run which illustrates the Z resolution of the detector system. It shows that the counter telescope permits yields of individual atomic numbers to be extracted up to about $Z=35$. However, for the bulk of the data the statistical accuracy was less than that of Fig. 6 and the data were integrated into intervals of width $\Delta Z=4$. Figure 7 shows a contour plot of Ar+Ag data in the E-ΔE plane. Dotted curves divide the fission events into regions characterized by different average Z values. The dotted curves were generated using the known thickness of the ΔE detector together with the tables of Northcliffe and Schilling.[11] It was assumed that all fragments had the same Z/A ratio as the com-

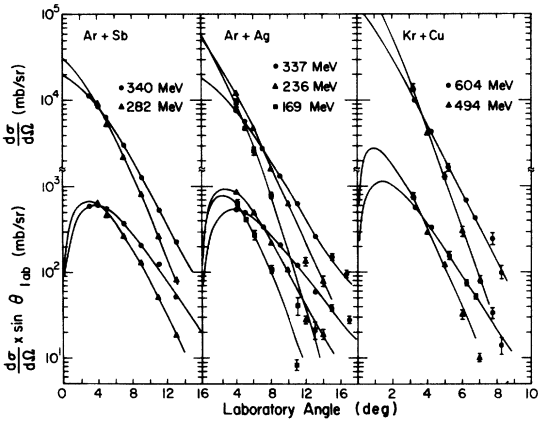

FIG. 5. Evaporation residue angular distributions. Curves were drawn arbitrarily through experimental results as discussed in the text. Lower points have been multiplied by the factor $\sin\theta$.

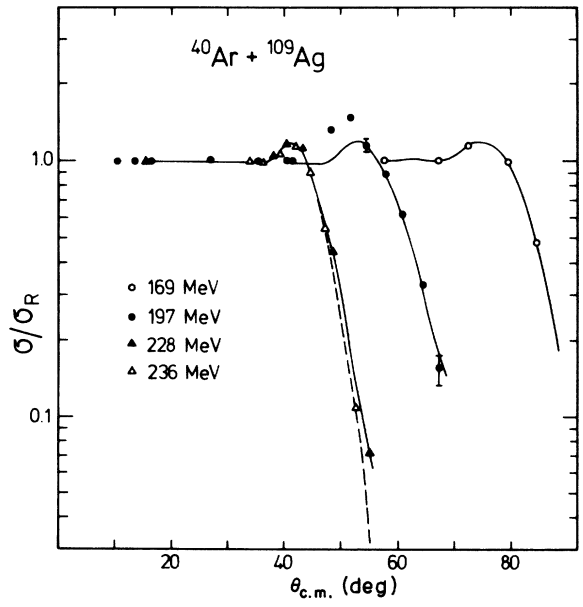

FIG. 4. Elastic scattering angular distributions with optical model fits using parameters given in Table II.

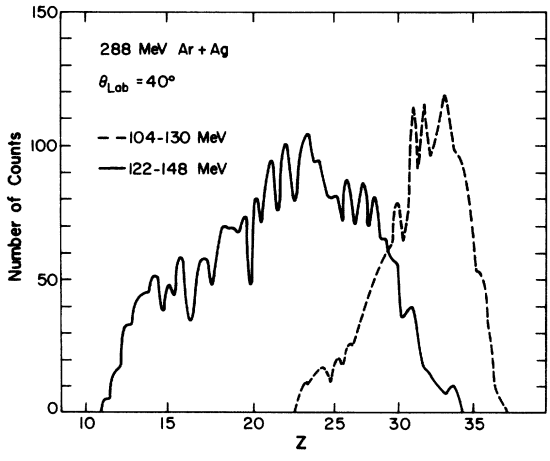

FIG. 6. Intensity versus ΔE distributions from one run. Ionization has been converted to atomic number as discussed in the text. The solid curve is for the lower Z region of the fissionlike yield curve for ions with energies between 122 and 148 MeV. The dashed curve is for the high Z distributions, with energies of 104 to 130 MeV.

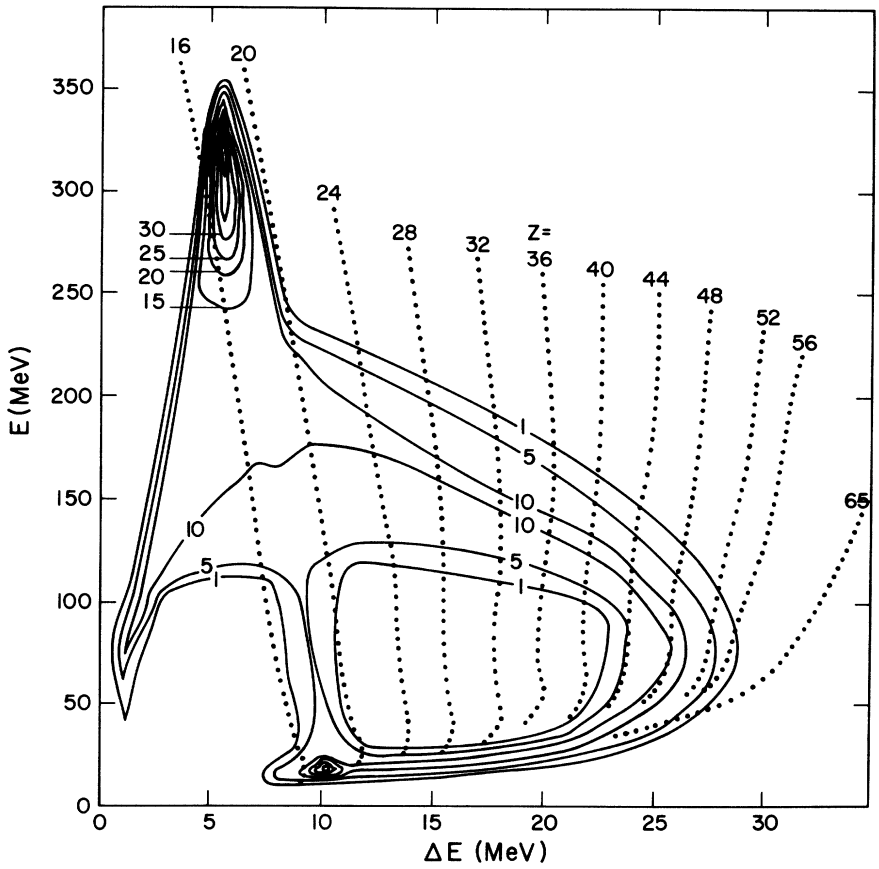

FIG. 7. Spectrum of the $^{40}Ar + ^{109}Ag$ reaction products in the E-ΔE plane. The solid contours represent intensity of the reaction products, and the dotted contours divide the area into regions of different average charge numbers. The argon energy is 337 MeV and the lab scattering angle is 21°.

pound system ^{149}Tb. Charge distributions were obtained by plotting the dotted curves of Fig. 7 on a transparent mask. The mask was used to overlay a computer display and to set movable line segments in the computer display to match the Z contours. For each laboratory angle the computer summed the events between the line segments and also calculated the corresponding average E and ΔE energies. These energies were used to transform the data in each Z interval into center of mass cross section.

Angular distributions for different fissionlike product yields are shown in Fig. 8. Yields for specific Z groups were obtained by drawing curves of the limiting form for a compound fission reaction, $1/\sin\theta$, through the points; in so doing, the points near 90° were weighted more heavily. Experimental results for products near symmetric fission for ^{40}Ar-induced reactions seem to follow the $1/\sin\theta$ angular distribution; the lower Z products in some cases seem to be more steeply forward peaked than the $1/\sin\theta$ distribution. Since yields of Fig. 9 were determined by integration of the $1/\sin\theta$ curves, the low Z product yields could be underestimated at forward angles. This error may be partially compensated by an overestimate at angles greater than 90°. Yields of these products are in reasonably good agreement with integration of yields reported by Thompson *et al.*[12]

The resulting yield-charge distributions are shown in Fig. 9. It may be seen that for the case of $^{40}Ar + ^{109}Ag$, there seem to be two groups of products; one is consistent with symmetric fission of a $Z \simeq 64$ compound nucleus, the other corresponds to products centered about $Z = 18$. This, coupled with the forward peaking (see Fig. 8) of the products near $Z = 18$, suggests that these yields are due to a mechanism which is qualitatively new in heavy ion reactions and has been called by various authors "strongly damped collisions," "deep inelastic transfer," and "quasi-fission."[13,14] Some forward peaking is also observed for the $^{84}Kr + ^{65}Cu$ yields for $Z \simeq 30$, sug-

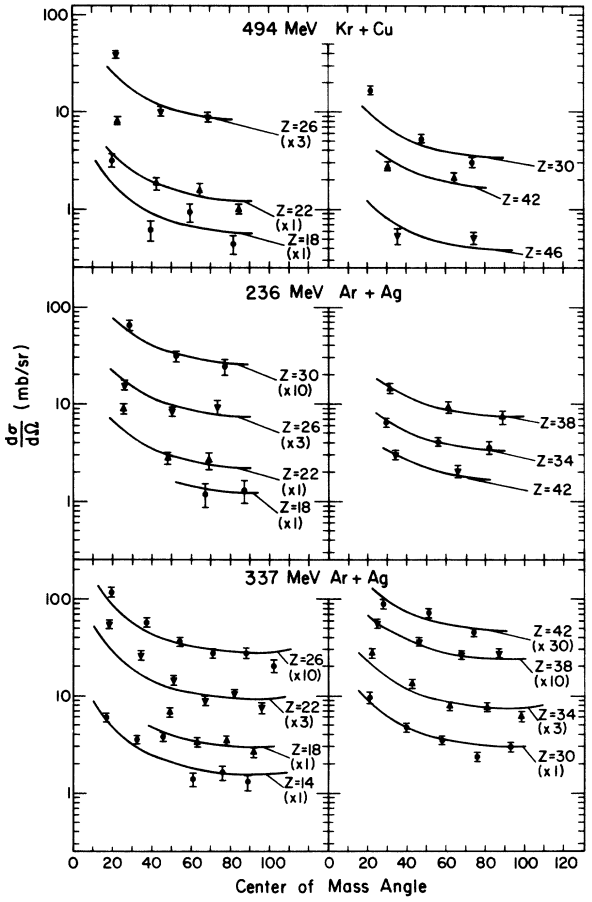

FIG. 8. Angular distributions of fission/quasifission fragments. Yields have been integrated in bins containing four atomic numbers. The solid curves are of the form $1/\sin\theta$; they have been drawn with a weighting towards the points at 90°.

gesting that much of these yields may also be due to a quasifission, rather than an equilibrium fission mechanism.

Symmetric curves have been drawn through the fissionlike yields of $^{84}Kr + ^{65}Cu$ with symmetry about $Z = 32$. These yields contain contributions from both fission and quasifission which cannot be separated in any unique manner using the present results. For the $^{40}Ar + ^{109}Ag$ yields, the high Z yields were used with an assumed symmetry about $Z = 32$ to estimate a symmetric fission yield. The smooth curve so drawn (Fig. 9) was subtracted from the lower yields in order to get the curves which are identified as quasifission. Fission yields reported in Table I were obtained as one-half the area under the symmetric fission curves. Yields identified as quasifission in Table I for $^{40}Ar + ^{109}Ag$ were obtained by integrating under the quasifission curves. Since the partners of the light fragments are not included in this inte-

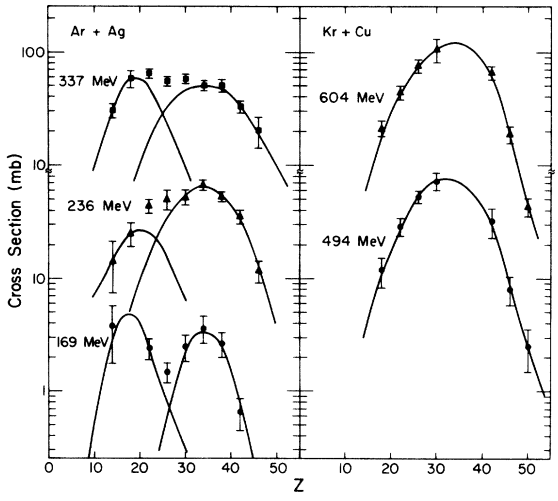

FIG. 9. Yield-charge distributions for reactions of $^{40}Ar + ^{109}Ag$ and $^{84}Kr + ^{65}Cu$. Laboratory energies are indicated on the figure. Resolution of the $^{40}Ar + ^{109}Ag$ data into fission and quasifission components is discussed in the text.

gration, no division by two was made. For these reactions the light particles ($Z \sim 18$) are predominately forward so that heavy partners are at large angles with low energy and would generally have been missed in our experiment. Yields for the $^{84}Kr + ^{65}Cu$ reactions were integrated and divided by two, since both partners were detectable.

Average kinetic energies as a function of charge

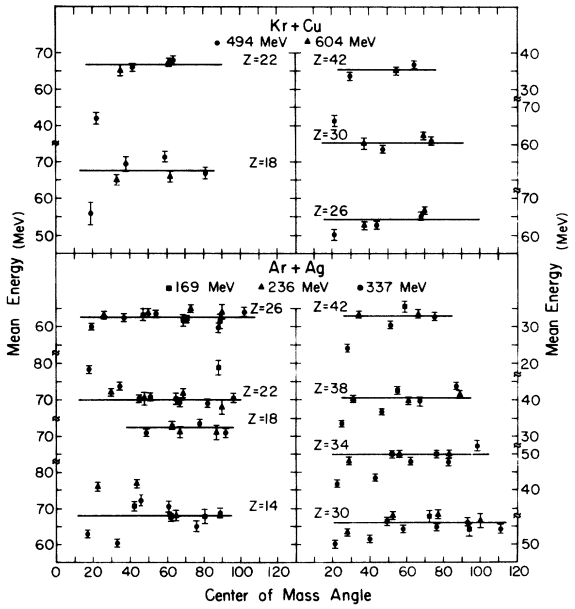

FIG. 10. Average fragment kinetic energy as a function of angle. Lines of zero slope have been arbitrarily drawn through the experimental points as a visual guide.

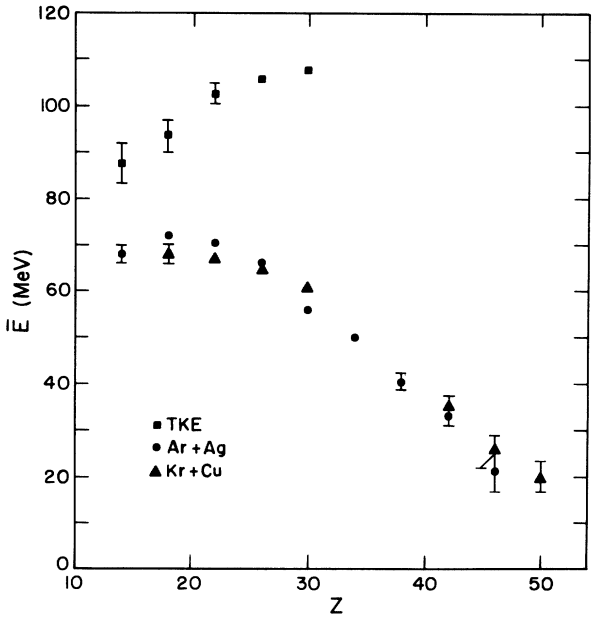

FIG. 11. Average and total kinetic energy as a function of fragment charge. Values are experimental results, uncorrected for light particle evaporation. Squares represent total kinetic energies by assuming reflection about $Z = 32$, using average of results for Kr- and Ar-induced reactions.

and center of mass angle are summarized in Fig. 10 for results for both Ar- and Kr-induced reactions. As stated previsouly, both systems make the ^{149}Tb compound nucleus or composite system. At center of mass angles greater than ~50° the kinetic energy for fixed charged division seems to be approximately independent of the target-projectile choice and isotropic in angle to within the experimental uncertainties as shown also in Figs. 10 and 11. At forward angles for ^{40}Ar + ^{109}Ag the fragment kinetic energies tend to be higher than average for low Z (14–22) and lower than average for high Z (30–42). Whether these deviations are characteristic of the quasifission process or simply an artifact of the experimental system or c.m. transformation is not clear. In general, the forward angle fission measurements are more difficult because of the presence of intense elastic scattering and of fusion products of light element impurities. Total kinetic energies are quite independent of projectile with the results shown in Fig. 11 representing an average of Ar and Kr results, with reflection about $Z = 32$. The results in Fig. 11 are taken from data shown in Fig. 10 weighted by the large angle regions, and, therefore, these results should be most characteristic of equilibrium fission and do not give significant information on possible differences in the total kinetic energy release for quasifission. The average total kinetic energy for symmetric fission found in this work was 104 ± 4 MeV. Correcting for particle emission (estimating 10 particles emitted from the fragments with 120 MeV of excitation) gives 111 ±4 MeV for the original average fragment total kinetic energy. This measured total kinetic energy release of 111 ± 4 MeV agrees well with the value of 108 MeV from the empirical systematics of Viola[15] and Plasil, Ferguson, and Pleasonton.[16] The value can also be compared with a theoretical liquid drop prediction of 102.5 MeV from Davies *et al.*[17] This theoretical value is for zero angular momentum and a viscosity coefficient $\mu = 0.015$ TP. The ~8.5 MeV measured increase over the expected theoretical value could be partially due to either of two effects[18]: (1) some of the rotational energy for our systems that are fissioning with $\bar{l} \sim 90$ ends up in kinetic energy of the fragments and (2) an increase in Coulomb energies could result from a systematic decrease in the radius parameter r_0 for lighter nuclei as predicted by Myers.[19]

IV. DISCUSSION

Much interest has centered in recent years on limiting values of angular momentum for the formation of a compound nucleus (fusion) or for formation of evaporation residue products.[20-23] Models for predicting limiting values of the angular momentum for fusion due to the entrance channel have been proposed and modified by several groups.[4,24-31] It is therefore of interest to summarize cross sections determined in this work in terms of angular momentum distributions; indeed this information was a prime reason for undertaking these experiments.

In heavy ion reactions of the type considered in this work, it has been common to characterize angular momentum limits, experimental and theoretical, in terms of a sharp cutoff limit. Comparisons of the sharp cutoff approach versus actual calculated distributions have been presented in Ref. 3 for the case of fission-evaporation calculations. In this work we assume the sharp cutoff model in the following discussions.

A. Evaporation residue cross sections

Using a recent statistical model calculation ER yields may be theoretically estimated as the portion of the fusion or compound nucleus cross section which survives fission competition. This calculation[4] includes competition between fission and light particle evaporation using an l dependent fission barrier. The result of the calculation for light nuclei is that fission dominates the deexcita-

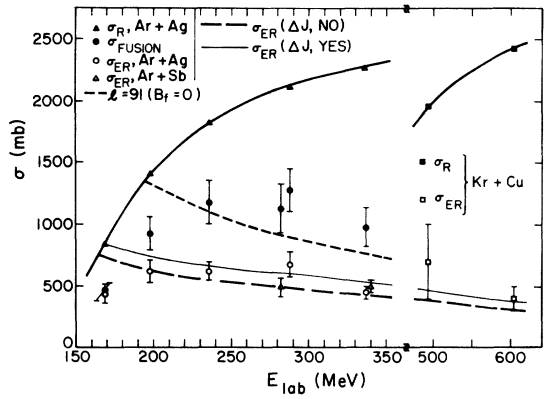

FIG. 12. Excitation functions for fusion, evaporation residue, and reaction cross sections. Significance of points and curves is indicated in the figure. Calculated limits for ER production and fusion limit $B_f^l = 0$ are also indicated and discussed in the text.

tion for high partial waves and evaporation for low partial waves. A more complete discussion of this model is given in Ref. 4. Calculations have been performed to estimate ER yields due to such an evaporation-fission mechanism. The angular momentum dependent fission barriers due to Cohen, Plasil, and Swiatecki[2] were used with a fission/evaporation competition model in the computer code ALICE.[3,4,32] Calculations were performed using a strict s-wave approximation (ΔJ no in Fig. 12), and with an approach in which neutrons and protons were each allowed to remove $2-3\hbar$ upon evaporation (ΔJ yes in Fig. 12).[4] These calculations may be seen to give very satisfactory agreement with experimental results at energies about 230 MeV, with no parameter variations having been performed. Standard parameter sets were used (liquid drop barriers, $a_f/a_n = 1$) as defined in Refs. 3 and 4. We conclude from the comparisons of Fig. 12 that the experimental ER yields are in very good agreement with the limits determined by the fission deexcitation model at energies for which the maximum angular momentum transfer exceeds the maximum angular momentum leading to ER products. At lower energies the surface transfer reactions compete at lower l values and reduce σ_{ER} below σ_R in the absence of fission competition.

The ER group for $^{40}Ar + ^{109}Ag$ has also had mass yields determined[33] by activation in a related work, and the distributions are found to be in very good agreement with the data presented in this paper. It should be noted that our yields of ER products of ^{121}Sb are considerably lower than previously published values but agree with the more recent results from Orsay.[34] Our results when used with fission yields measured at Orsay[35] give fusion cross sections near the limit where the fission barrier becomes zero, $B_f^l = 0$. The fusion cross sections will be discussed in the following subsection.

B. Fusion cross sections

The fusion cross section is given by the sum of the ER and fission cross sections; results are summarized in Table I. In taking the sum, it is required that only the equilibrium fission contribution be included, and not quasifission. The differentiation between these two alternatives is particularly uncertain for the case $^{84}Kr + ^{65}Cu$, since the mass division for quasifission and for symmetric fission could well be similar. Estimates of fusion cross sections for the reactions of $^{84}Kr + ^{65}Cu$ in Table I may, therefore, contain large noncompound cross section contributions and should be interpreted at best as upper limits.

Many suggestions have been made concerning the physical considerations which may determine the magnitude of fusion cross sections as a function of target and projectile atomic number and projectile energy. The requirements for fusion are presently thought to be as follows: First, a necessary condition is that the one dimensional potential energy curve consisting of Coulomb plus nuclear plus centrifugal contributions must have a relative maximum, and that the incident ion energy be in excess of this maximum. Second, that there exist sufficient dissipative forces to reduce the relative velocities of the target and projectile to a point that fusion can take place if otherwise possible. Third, that the dynamic path between the entrance channel configuration and the compound nucleus will pass within the saddle point shape for fission. These general considerations can be used[36] to divide the excitation energies into three broad regions: (I) At energies near and slightly above the Coulomb and fusion barriers the fusion process can be adequately described in terms of the penetrability through a one dimensional potential barrier and the relevant physical considerations concern whether for a particular l value the maximum in the potential energy surface is exceeded and whether there then exists a minimum and sufficient dissipative forces to trap the system and lead to fusion; (II) in an intermediate energy region for most l values the system is above the fusion barrier, but there is an additional restriction that the dynamic path of the system must pass within the fission saddle point for it to fuse to a compound nucleus; (III) at still higher energies one starts to excite the nucleus with even higher l waves for which the fission barrier has decreased to zero and there

is no compound system available in the usual sense. In the present work we have evidence for fusion proceeding in regions I and III and we will discuss these two regions separately. The number of experimental points and their accuracies do not allow any conclusions regarding possible fusion of the type in region II.

1. Fusion at low energies

From Fig. 12 we see that at the two lowest energies for the $^{40}Ar + ^{109}Ag$ case the fusion cross sections fall below the total reaction cross sections, and, similarly, the ER cross sections are lower than predicted. In this case the highest l values do not have enough energy to overcome the one dimensional fusion barrier, but they do have enough energy to bring the nuclei together close enough so that quasielastic reactions can occur (note that at 169 MeV the quasifission cross section is also small so that presumably ~40% of the total reaction cross section must be going into these quasielastic processes).

In order to investigate the low energy region more quantitatively, fusion excitation functions have been analyzed in terms of a classical sharp cutoff model, in which it is assumed that all target and projectile energies are in the potential or kinetic mode, with no internal excitations.[5] The fusion cross section[5] resulting from this model is

$$\sigma = \pi R^2 (1 - V/E) ,$$

where R is an effective interaction radius and E and V the kinetic energy and interaction barrier height. From Eq. (4), so far as the conservative forces assumptions are valid, it may be seen that a graph of σ versus $1/E$ should allow a determination R and V from slope and intercept, respectively. Such an analysis is shown in Fig. 13 using total reaction cross sections from the elastic scattering results and fusion cross sections (all for the $^{40}Ar + ^{109}Ag$ system). These analyses yield a reaction barrier of 139 ± 3 MeV and a fusion barrier height of 148 ± 6 MeV. The reaction barrier may actually be an upper limit because of the difficulties involved in separating all the quasielastic events in the elastic measurement which were used to determine σ_R. This analysis also gives interaction radii of 10.9 ± 0.9 and 12.4 ± 0.4 fm for fusion and quasielastic reaction, respectively. The interaction radius for quasielastic reactions is consistent with the value of ~12.0 fm determined from the quarter-point analyses of the elastic scattering at 169–236 MeV (see Sec. III A).

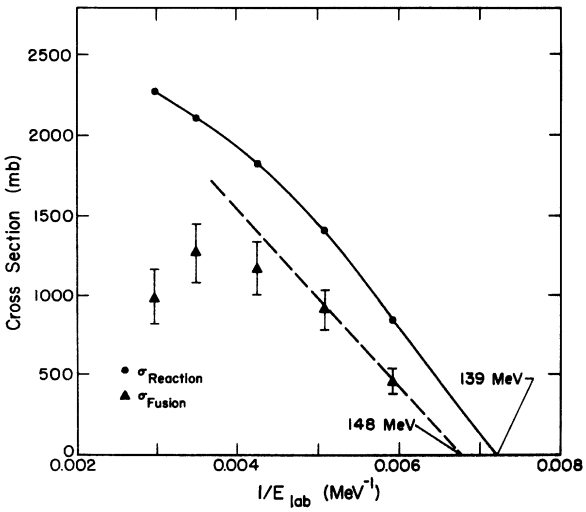

FIG. 13. Analysis for reaction and fusion barrier heights and radii in the classical sharp cutoff limit. The basis of these analyses is discussed in the text.

In the center of mass system our reaction and fusion barriers are 102 and 108 MeV, respectively, and they can be compared with theoretical calculations of Nix and co-workers[36,37] which give 98.4 and 104.0 MeV, respectively. In particular, the measured difference of 6 ± 4 MeV agrees well with a calculated difference of 5.6 MeV. Similarly, the measured reaction and fusion radii (12.4 and 10.9 fm) can be compared with theoretical values of 11.9 and 10.3 fm, respectively. Again the measured difference in radii 1.5 ± 0.9 fm is in reasonable agreement with the predicted difference of 1.6 fm. While results of analyses of our experimental data may be seen to be in qualitative agreement with theory, the large error limits on the experimental determinations do not allow an unequivocal test of the theoretical predictions.

2. Fusion at high energies

In Fig. 12 the experimental fusion cross sections are also compared with predictions[2] for the angular momentum limit at which the fission barrier goes to zero. It is seen that for the high energies ($E_{lab} \geq 236$ MeV) the measured values tend to exceed this limit. An average of the highest two energies from the Ar + Ag data give $l_{crit} = 105 \pm 6\hbar$ compared with the liquid drop values of $l_{B_f=0} = 91\hbar$. The increase of the measured l_{crit} value over the calculated liquid drop value could be due, on the one hand, to the inclusion in the fission cross sections of components for which $B_f = 0$ but which apparently have long enough lifetime to equilibrate mass and energy distributions and become indistinguishable from normal compound fission. On the other hand, the liquid drop calculations may underestimate $l_{B_f=0}$ because of the neglect of diffusivity[38] in the potentials used or

the intrinsic angular momentum of excited nucleons might slightly extend the angular momentum for which $B_f > 0$ in an excited nucleus.[23]

In this picture of fusion reactions at high energy the cross section involved in reactions for which $l > l_{B_f=0}$ could involve significant interpenetration of the two nuclei, but since there does not exist any quasistable compound nucleus configuration these states must decay without equilibrating. It seems reasonable to conclude that these reactions give rise to the "quasifission" or "deep inelastic" components which involve a considerable loss of energy but insufficient time to equilibrate the mass division. It should be noted that the "quasifission" observed in Ar+Ag reactions is strongly forward peaked and similar to the Ar+Th discussed by Wilczynski[26] but quite different from the grazing peak angular distributions observed for deep inelastic collisions with Kr projectiles on heavy targets.[39-42] Thus, in this particular region, Ar+Ag, the l_{crit} values seem to be qualitatively consistent with the liquid drop limit for compound nucleus formation and there is no *a priori* need to consider one of the many current models which invoke a dissipative force in a one dimensional collision model in order to calculate l_{crit}. Further discussion of this point is presented in the following subsection.

3. *Comparison with one dimensional models for fusion*

Many current models of the limiting angular momentum for fusion are based on a one dimensional potential energy curve (nuclear attractive force versus Coulomb and centrifugal forces) with a requirement that there be a region for which the one dimensional two-body potential have a relative minimum.[25,26] Some models add a dissipative force to describe the trapping of the two nuclei in the relative minimum.[27,31] For our cases many of the calculations give similar results and in Fig. 14 we present a comparison of our cross sections with the predictions of the models of Bass[27] and Gross.[28] It is seen that the agreement is reasonably good. We believe that for our relatively light systems this is the correct type of model to compare with at low energies, but as discussed above at the highest energies the liquid drop limit may be the more relevant parameter.

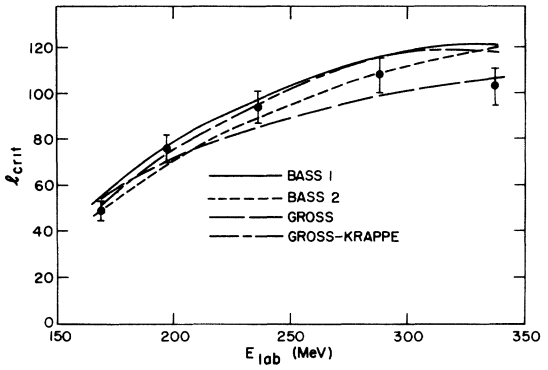

FIG. 14. Comparison of experimental l_{crit} values from Table I for the $^{40}Ar + ^{109}Ag$ reaction with theoretical predictions from Bass (Ref. 27) and Gross *et al.* (Ref. 28). The curves labeled "Bass 1" and "Bass 2" refer, respectively, to the use of Woods-Saxon and exponential form factors in the nuclear potential.

V. SUMMARY

In this paper we have presented experimental cross sections for three main catagories of reaction products and estimated total reaction cross sections from ^{40}Ar bombardment of ^{109}Ag and ^{121}Sb and from ^{84}Kr bombardment of ^{65}Cu. The products measured are evaporation residues, equilibrium fission, and a fissionlike group called deep inelastic transfer or quasifission. In all cases the evaporation residue products can be unambigously identified in the experimental data, but in the ^{84}Kr bombardments the accuracy of the cross sections are seriously limited by our experimental inability to measure at angles forward of 3° where a majority of the cross section occurs. For the ^{40}Ar reactions on ^{109}Ag it is shown that the total cross section as a function of Z can be approximately separated into two components (equilibrium and quasifission) by assuming that the equilibrium fission has a symmetric Z distribution. Then total fusion cross section can be estimated as the sum of the ER and equilibrium fission cross sections. In the ^{84}Kr data it is not possible to perform this separation between equilibrium and quasifission because of the expected similarity in the Z distributions for the two cases. In all cases we find that a large fraction (15–40%) of the total reaction cross section is unaccounted for and presumably goes into quasielastic events which were not investigated in the present experiment.

The ER and fusion yields for the $^{40}Ar + ^{109}Ag$ system are compared with predictions of various one dimensional heavy ion reaction models[27,28] and with simple predictions of fusion for a rotating liquid drop[2] followed by compound nucleus decay via particle emission and equilibrium fission.[32] These comparisons show the fusion cross sections (or l_{crit} values) are in good agreement with predictions of the one dimensional models at energies near the fusion barrier. At high energies the results can be more simply understood in terms of the rotating liquid drop model. A schematic comparison of the 337 MeV $^{40}Ar + ^{109}Ag$ data compared with predictions of the liquid drop mod-

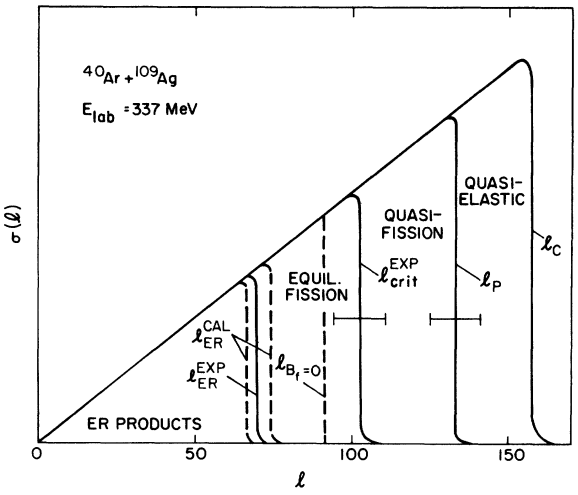

FIG. 15. A schematic illustration of the experimental and theoretical components in the cross section as a function of angular momentum in the entrance channel for the $^{40}Ar + ^{109}Ag$ reaction at 337 MeV. This model assumes a sharp cutoff in l when assigning different processes to different regions of l. Solid vertical lines with horizontal error bars indicate experimental quantities from Table I. Dashed vertical lines indicate theoretical limits as described in the text.

el with standard compound nucleus deexcitation is shown in Fig. 15. In Fig. 15 the various cross sections are converted to maximum l values using a sharp cutoff approximation assuming that the lowest l values produce ER products up to a maximum value l_{ER}, equilibrium fission occurs primarily for $l_{ER} < l < l_{crit}$ and quasifission dominates in the region $l_{crit} < l < l_p$ with quasieleastic reactions dominating the very highest l values which correspond to peripheral collisions. In this picture it is seen that the quasifission products come from a region of l values for which no barrier exists for normal fission and, therefore, there is no compound nucleus available in the traditional sense. This assignment of the quasifission reactions to the region $l > l_{B_{f=0}}$ and equilibrium fission to the region $l > l_{ER}$ is also consistent with the 169 MeV results where $l_c < l_{ER}$ and both the equilibrium and quasifission cross sections are seen to be very small.

The interpretation suggested in Fig. 15 for the decomposition of the evaporation residue, fusion, and quasifission cross sections is not consistent with the recent hypothesis of Lefort[43, 44] where he suggests that the quasifission reactions are competing strongly in the region of the very lowest l waves. In particular, he suggests that for the cases $^{84}Kr + ^{74}Ge$ and $^{40}Ar + ^{118}Sn$ the quasifission reactions may be dominated by $l \leq 45$ for the ^{84}Kr case and $l \leq 20$ for the ^{40}Ar case. This interpretation comes primarily from attempts to understand the observed excitation functions[34] for xn reactions in these cases. Our data do not seem to fit easily into such an interpretation and the assumption that the quasifission comes from the region $l > l_{B_{f=0}}$ appears to be much more reasonable. The major aspects of our results which are at variance with the Lefort proposal are (1) ER cross sections agree well with calculations from the Blann-Plasil model,[3,4] whereas if the Lefort proposal were correct the calculations should be compared with $\sigma_{ER} + \sigma_{QF}$. Particularly for $^{84}Kr + ^{65}Cu$ if we assumed that the first 45 partial waves go to quasifission,[44] then $\sigma_{ER} + \sigma_{QF} = 550 \pm 100$ mb which is considerably larger than the calculations of 300–375 mb; (2) for $^{40}Ar + ^{109}Ag$ the measured σ_{QF} increases from 45 to 700 mb as the projectile energy increases from 169 to 337 MeV, whereas the Lefort hypothesis that quasifission comes mostly from the region $l \lesssim 20$ would predict σ_{QF} decreasing from ~80 to ~40 mb in this energy region; (3) if we assume that l_{crit} should be calculated from the sum $\sigma_{fusion} + \sigma_{QF}$ as suggested by Lefort instead of from σ_{fusion} alone as we suggest above, then at the highest energies we would get $l_{crit} \sim 130\hbar$ for $^{40}Ar + ^{109}Ag$ (337 MeV) and $l_{crit} \sim 150\hbar$ for $^{84}Kr + ^{65}Cu$ (604 MeV). These values seem unreasonably large when compared with the Cohen, Plasil, and Swiatecki calculations of $l_{B_{f=0}} = 91\hbar$.

VI. ACKNOWLEDGMENTS

It is a pleasure to acknowledge many useful discussions with J. R. Nix, W. J. Swiatecki, and J. R. Huizenga. We are grateful to the entire group at the Lawrence Berkeley Laboratory Super heavy ion linear accelerator for help during the operation of these experiments. We further express our appreciation to J. C. Gursky for preparation of the many targets used in these experiments. We would like to thank R. Bass and D. H. E. Gross for supplying predictions of l_{crit} for our cases using their theoretical models.

*Work supported by the U. S. Energy Research and Development Administration.
†Work supported by a grant from the National Science Foundation.

[1] V. Weisskopf and D. H. Ewing, Phys. Rev. 57, 472 (1940).
[2] S. Cohen, F. Plasil, and W. J. Swiatecki, Ann. Phys. (N.Y.) 82, 557 (1974).
[3] M. Blann and F. Plasil, Phys. Rev. Lett. 29, 303 (1972).
[4] F. Plasil and M. Blann, Phys. Rev. C 11, 508 (1975).

[5]H. H. Gutbrod, W. G. Winn, and M. Blann, Nucl. Phys. A213, 267 (1973).
[6]J. S. Blair, Phys. Rev. 95, 1218 (1954).
[7]It should be noted, however, that the use of this form for η neglects nuclear effects so that the values obtained from this analysis for R_C are Coulomb radii which are generally larger than radii extracted from optical model analyses. This point is discussed in detail in: H. H. Gutbrod, M. Blann, and W. G. Winn, Nucl. Phys. A213, 285 (1973).
[8]E. H. Auerbach and C. E. Porter, in *Proceedings of the Third Conference on Reactions Between Complex Nuclei,* edited by A. Ghiorso, (Univ. of Calif. Press, Berkeley, 1963), p. 19.
[9]J. B. Natowitz, Phys. Rev. C 1, 623, 2157 (1970); J. B. Natowitz, E. T. Chulick and M. N. Namboodiri, *ibid.* 6, 2133 (1972).
[10]H. H. Gutbrod, F. Plasil, H. C. Britt, B. H. Erkkila, R. H. Stokes, and M. Blann, in *Proceedings of the Third International Atomic Energy Symposium on the Physics and Chemistry of Fission, Rochester, 1973;* (International Atomic Energy Agency, Vienna, Austria, 1974), Vol. II, p. 309.
[11]L. C. Northcliffe and R. F. Schilling, Nucl. Data A7, 233 (1970).
[12]S. G. Thompson, L. G. Moretto, R. C. Jared, R. P. Babinet, J. Galin, M. M. Fowler, R. C. Gatti, and J. B. Hunter, Lawrence Berkeley Laboratory Report No. LBL-2940, 1974 (unpublished).
[13]F. Hanappe, C. Ngo, J. Peter, and B. Tamain, in *Proceedings of the Third International Atomic Energy Symposium on the Physics and Chemistry of Fission, Rochester, 1973* (see Ref. 10), Vol. II, p. 289; M. Lefort, Y. LeBeyec, and J. Peter, Report No. IPNO-RC-73-04, 1973 (unpublished), presented at XI Winter Meeting on Nuclear Physics, Villars, 1973.
[14]Search and Discovery, Physics Today, Dec. 1974; F. Hanappe, M. Lefort, C. Ngo, J. Peter, and B. Tamain, Phys. Rev. Lett. 32, 738 (1974).
[15]V. E. Viola, Jr., Nucl. Data 1, 391 (1966).
[16]F. Plasil, R. L. Ferguson, and F. Pleasonton, in *Proceedings of the Third International Atomic Energy Symposium on Physics and Chemistry of Fission, Rochester, 1973* (see Ref. 10), Vol. II, p. 319.
[17]K. T. R. Davies, S. E. Koonin, J. R. Nix, and A. J. Sierk, Los Alamos Scientific Laboratory Report No. LA-UR-75-5 (unpublished), presented at the International Workshop III on Gross Properties of Nuclei and Nuclear Excitations, Hirschegg, Kleinwalsertal, Austria, January 13–18, 1975.
[18]J. R. Nix (private communication).
[19]W. D. Myers, Lawrence Berkeley Laboratory Report No. LBL-3428 (unpublished).
[20]L. Kowalski, J. C. Jodogne, and J. M. Miller, Phys. Rev. 169, 894 (1968).
[21]M. Lefort, Incomplete Fusion Reactions Between Heavy Ions, Europhysics Conference on Nuclear Interactions at Medium and Low Energies, Harwell, 1975 (unpublished).
[22]M. Blann, in *Proceedings of the International Conference on Nuclear Physics, Munich 1973,* edited by H. J. Mang and J. De Boer, (North-Holland/American Elsevier, New York, 1974), Vol. II, p. 657; M. Blann, Proceedings of the VIth Masurian School in Nuclear Physics, Nukleonika 19, 203 (1974).
[23]J. R. Huizenga, Proceedings of the VIIth Masurian School in Nuclear Physics, Nukleonika 20, 291 (1975).
[24]B. N. Kalinkin and I. Z. Petkov, Acta Phys. Pol. 25, 265 (1964).
[25]R. Basile, J. Galin, D. Guerreau, M. Lefort, and X. Tarrago, J. Phys. 33, 9 (1972).
[26]J. Wilczynski, Nucl. Phys. A216, 386 (1973); Phys. Lett. 47B, 484 (1973).
[27]R. Bass, in *Proceedings of the International Conference on Nuclear Physics, Munich, 1973* (see Ref. 22), Vol. 1, p. 614; Phys. Lett. 47B, 139 (1973); Nucl. Phys. A231, 45 (1974); and private communication.
[28]D. H. E. Gross and H. Kalinowski, Phys. Lett. 48B, 302 (1974); D. H. E. Gross, H. Kalinowski, and J. N. De, in *Proceedings of the Symposium on Classical and Quantum Mechanical Aspects of Heavy Ion Collisions, Heidelberg, 1974* (Springer-Verlag, Berlin, 1975), p. 194; J. N. De, D. H. E. Gross, and H. N. Kalinowski, Hahn Meitner Institute (unpublished); and private communication.
[29]J. Bondorf, M. Sobel, and D. Sperber, Phys. Rev. C 11, 1265 (1975).
[30]J. Randrup, W. J. Swiatecki, and C. T. Tsang, Phys. Scripta (to be published).
[31]E. Seglie, D. Sperber, and A. Sherman, Phys. Rev. C 11, 1227 (1975).
[32]M. Blann and F. Plasil, ALICE, a nuclear evaporation code, Report No. COO-3494-10, 1973 (unpublished).
[33]M. Hille, P. Hille, H. H. Gutbrod, and M. Blann, Nucl. Phys. A252, 496 (1975).
[34]H. Gauvin, Y. LeBeyec, and N. T. Porile, Nucl. Phys. A223, 103 (1974); H. Gauvin, Y. Lebeyec, M. Lefort, and R. L. Hahn, Phys. Rev. C 10, 722 (1974); H. Gauvin, D. Guerreau, Y. Lebeyec, M. Lefort, F. Plasil, and X. Tarrago, Phys. Lett. 58B, 163 (1975).
[35]T. Tamain, C. Ngo, J. Peter, and F. Hanappe, Nucl. Phys. A252, 187 (1975).
[36]A. J. Sierk and J. R. Nix, Bull. Am. Phys. Soc. 20, 69 (1975); J. R. Nix (private communication).
[37]H. J. Krappe and J. R. Nix, in *Proceedings of the Third International Atomic Energy Symposium on Physics and Chemistry of Fission* (see Ref. 10), Vol. I, p. 159.
[38]J. R. Nix (private communication).
[39]K. L. Wolf, J. P. Unik, J. R. Huizenga, J. R. Birkelund, H. Freiesleben, and V. E. Viola, Phys. Rev. Lett. 33, 1105 (1974).
[40]J. Péter, C. Ngô, and B. Tamain, J. Phys. (Paris) Lett. 36, 23 (1975).
[41]B. Gatty, D. Guerreau, M. Lefort, X. Tarrago, J. Galin, B. Cauvin, J. Girard, and H. Nifenecker, Nucl. Phys. A253, 511 (1975).
[42]R. Vandenbosch, M. P. Webb, and T. D. Thomas, Univ. of Washington (unpublished).
[43]M. Lefort, Phys. Rev. C 12, 686 (1975).
[44]M. Lefort, in Heavy Ion Collisions, edited by R. Bock (North-Holland, Amsterdam, to be published).